Using scattering theory to compute invariant manifolds and numerical results for the laser-driven Hénon-Heiles system

Daniel Blazevski and Jennifer Franklin

Citation: Chaos **22**, 043138 (2012); doi: 10.1063/1.4767656
View online: http://dx.doi.org/10.1063/1.4767656
View Table of Contents: http://scitation.aip.org/content/aip/journal/chaos/22/4?ver=pdfcov
Published by the AIP Publishing

Using scattering theory to compute invariant manifolds and numerical results for the laser-driven Hénon-Heiles system

Daniel Blazevski[a] and Jennifer Franklin
Department of Mathematics, University of Texas at Austin, 1 University Station C1200, Austin, Texas 78712, USA

(Received 18 June 2012; accepted 26 October 2012; published online 11 December 2012)

Scattering theory is a convenient way to describe systems that are subject to time-dependent perturbations which are localized in time. Using scattering theory, one can compute time-dependent invariant objects for the perturbed system knowing the invariant objects of the unperturbed system. In this paper, we use scattering theory to give numerical computations of invariant manifolds appearing in laser-driven reactions. In this setting, invariant manifolds separate regions of phase space that lead to different outcomes of the reaction and can be used to compute reaction rates. © *2012 American Institute of Physics*. [http://dx.doi.org/10.1063/1.4767656]

In this paper, we implement numerically the theoretical ideas of Blazevski and de la Llave (2011) using the laser-driven Hénon-Heiles system introduced in Kawai *et al.* (2007). The ideas of this paper are robust and can be used for any system subject to a time-dependent perturbation localized in time. Using the intertwining relations, scattering theory yields a time-dependent conjugacy between the perturbed and unperturbed systems. Assuming one has the relevant invariant manifolds for the unperturbed system, we exploit the conjugacy to compute the corresponding objects for the perturbed system. The algorithm used in this paper to compute invariant manifolds is an alternative to the use of time-dependent normal form theory used in Kawai *et al.* (2007) and is readily parallelizable.

I. INTRODUCTION

A theoretical framework describing the use of scattering theory to compute invariant manifolds for classical systems subject to a time-dependent perturbation that is localized in time and space was given in Blazevski and de la Llave (2011). In particular, the laser-driven Hénon-Heiles system introduced in Kawai *et al.* (2007) was shown to fit within the framework in Blazevski and de la Llave (2011). However, numerical computations in Blazevski and de la Llave (2011) were not given, and the goal of this paper is to give numerical results that illustrate how one can compute time-dependent invariant objects using scattering theory. We focus on the laser-driven Hénon-Heiles system since it fits within the framework where scattering theory applies and it is also of physical interest.

Scattering theory gives a way to relate the perturbed manifolds to the unperturbed manifolds. If the perturbation is localized enough in time (e.g., the perturbation considered in Kawai *et al.* (2007) was compactly supported in time, and this fits within the framework of Blazevski and de la Llave (2011)), then we have the existence the wave maps $\Omega_{\pm}^{t_0}$. We postpone the definition of the wave maps until Sec. II, for now, we merely mention that they are diffeomorphisms of the phase space. As we recall in Sec. II, if M is an invariant manifold for the unperturbed system (e.g., a fixed point, periodic orbit, or stable and unstable manifolds) then the families $N_{t_0}^+$ and $N_{t_0}^-$ defined by

$$N_{t_0}^{\pm} := (\Omega_{\pm}^{t_0})^{-1}(M) \tag{1}$$

are time-dependent invariant manifolds for the perturbed flow. Thus, provided one has the unperturbed objects computed, then the computation of the corresponding perturbed objects is reduced to computing the inverse wave maps $(\Omega_{\pm}^{t_0})^{-1}$. This yields a geometric, efficient method that is highly parallelizable since one merely needs to compute a fixed diffeomorphism $(\Omega_{\pm}^{t_0})^{-1}$ to an array of points corresponding to the unperturbed manifolds.

The methods of this paper are of particular interest in chemistry, since invariant manifolds has proved to be useful to compute reaction rates in transition state theory (see, for example, Bartsch *et al.* (2012); Waalkens *et al.* (2008)). The computation of physically relevant quantities from transition state theory such as the branching ratio has been improved using invariant manifolds. The goal of this paper is not to compute quantities like reaction rates or branching ratios, but to show how one can compute the relevant invariant manifolds that have been used to compute such quantities.

In Sec. II, we review the theory developed in Blazevski and de la Llave (2011) with an emphasis on the numerical implementation of the theory. As a simple illustration of the theory, we show how it applies to perturbations of autonomous two-dimensional systems linear systems. In Sec. III, we apply the theory thus developed to a problem in transition state theory, namely to the laser-driven Hénon-Heiles system considered in Kawai *et al.* (2007).

II. BACKGROUND FROM TIME-DEPENDENT SCATTERING THEORY

In this section, we review time-dependent classical scattering theory, with an emphasis on applying the theory for the

[a]Present address: Institute for Mechanical Systems, Department of Mechanical and Process Engineering, ETH Zurich, Tannenstrasse 3, 8092 Zurich, Switzerland. Electronic mail: blazevski@imes.mavt.ethz.ch.

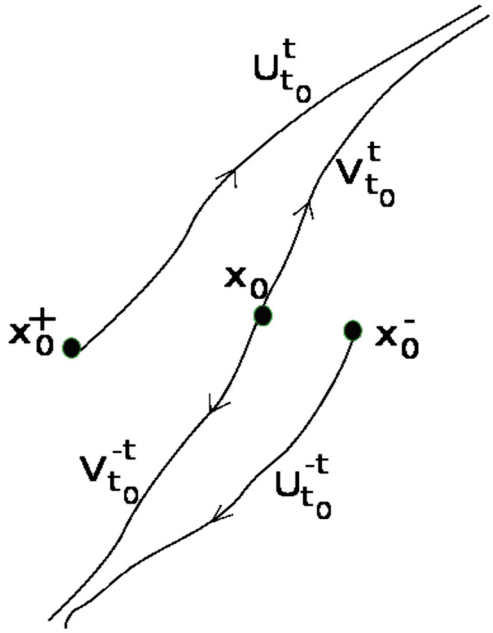

FIG. 1. Geometric interpretation of the wave maps. Given an initial condition x_0 for the perturbed flow $V^t_{t_0}$, the point $x_0^+ := \Omega^{t_0}_+$ (resp. $x_0^- := \Omega^{t_0}_-$) is the unique point whose orbit under the unperturbed flow $U^t_{t_0}$ is asymptotic in the future (resp. past) to the orbit of x_0. Reprinted with permission from Blazevski, D. and de la Llave, R., "Time-dependent scattering theory for odes and applications to reaction dynamics," J. Phys. A: Math. Theor. **44**, 195101 (2011). Copyright 2012 IOP Publishing.

numerical computation of invariant manifolds for systems subject to a perturbation that is localized in time and in space. Many, but not all, of the topics have been developed in Blazevski and de la Llave (2011). In particular, we further explore the dynamics of the perturbed system and a numerical method based on scattering theory to compute invariant manifolds, and we illustrate the theory with an example of a time-dependent perturbation of a two-dimensional hyperbolic linear flow. Our exposition on the wave maps and scattering theory is brief since a thorough treatment consisting of rigorous mathematical results and comparisons to existing literature on scattering theory were given in Blazevski and de la Llave (2011).

According to Blazevski and de la Llave (2011), scattering theory for time-dependent vector fields considers an ODE

$$\frac{d}{dt}X(t) = \mathcal{V}(X(t),t) = \mathcal{U}(X(t),t) + \mathcal{P}(X(t),t), \tag{2}$$

in Euclidean space subject to a time-dependent perturbation which is localized in time and space. Here, $\mathcal{U}$ is considered to be the unperturbed vector field and $\mathcal{P}(X,t)$ is the perturbation that is localized in time and space. We do not assume that $\mathcal{P}$ has small amplitude globally in space and time. We require that the perturbation amplitude decays in time, but is allowed to be arbitrarily large for transient period. Thus, standard perturbation theory does not apply since the amplitude can be large for a transient time. Let $U^t_{t_0}$ and $V^t_{t_0}$ represent the flows from t_0 to t of the unperturbed and perturbed vector fields, respectively. In particular, we have $U^t_{t_0} \circ U^{t_0}_s = U^t_s$ and $V^t_{t_0} \circ V^{t_0}_s = V^t_s$. The wave maps are then defined by

$$\Omega^{t_0}_\pm = \Omega^{t_0}_\pm(U,V) = \lim_{t\to\pm\infty} U^{t_0}_t \circ V^t_{t_0}. \tag{3}$$

The scattering map s^{t_0} is then defined as

$$s^{t_0} = \Omega^{t_0}_+ \circ (\Omega^{t_0}_-)^{-1}. \tag{4}$$

Wave maps provide a precise way of describing how the flow $V^t_{t_0}$ behaves like the flow $U^t_{t_0}$. Indeed, we have

$$U^{\pm T}_{t_0}(\Omega^{t_0}_\pm(X)) \approx V^{\pm T}_{t_0}(X), \tag{5}$$

for large $T > 0$. See Fig. 1 for a geometric illustration of Eq. (5). In Blazevski and de la Llave (2011), conditions are given on the flow $U^t_{t_0}$ and the vector field $\mathcal{P}$ for the wave maps to exist. The main idea is that the decay rate of $|\mathcal{P}|$ should be larger than the growth rate of $||DU^t_{t_0}||$. In this paper, our numerical results will be for $\mathcal{P}$ compactly supported in time, in which case the wave maps exist, are smooth, and are invertible (see Blazevski and de la Llave (2011) for details on when the wave maps exist in general, and Sec. II A for the case of compactly supported perturbations). It is important to note that these wave maps are for non-autonomous flows that depend on the starting time t_0.

Assuming that $\Omega^{t_0}_\pm$ are invertible and the limits defining them exist pointwise, we have the intertwining relations

$$\Omega^t_\pm \circ V^t_{t_0} = U^t_{t_0} \circ \Omega^{t_0}_\pm \tag{6}$$

yield a time-dependent conjugacy between $U^t_{t_0}$ and $V^t_{t_0}$. That the wave maps yield a conjugacy has been studied before in autonomous systems, the use scattering theory for autonomous classical systems has been used to study the local behavior near a hyperbolic fixed point in Nelson (1969) and was used to prove that certain systems, for example, the Calogero-Moser system, is integrable (Gutkin, 1985b, 1985a; Hubacher, 1989).

In this paper, our use of the time-dependent conjugacy is to take invariant objects of the unperturbed flow to corresponding time-dependent invariant manifolds for the perturbed flow. We recall that a *time-dependent invariant manifold* for the flow $V^t_{t_0}$ is a family of manifolds M_t parameterized by time that satisfy the invariance condition

$$V^t_{t_0}(M_{t_0}) = M_t. \tag{7}$$

The motivation for the computational results in this paper is the following general result from Blazevski and de la Llave (2011).

Theorem 1. *Suppose the wave maps $\Omega^{t_0}_\pm$ exist for the flows $U^t_{t_0}$ and $V^t_{t_0}$. If M_t is a time-dependent invariant manifold for $U^t_{t_0}$ then the families N^+_t and N^-_t of manifolds defined by*

$$N^\pm_t = (\Omega^t_\pm)^{-1}(M_t) \tag{8}$$

are time-dependent invariant manifolds for the flow $V^t_{t_0}$.

Theorem 1 yields a numerical method to compute invariant manifolds for the perturbed systems knowing the relevant manifolds for the unperturbed system. Indeed, given a time-dependent invariant manifold M_t for $U^t_{t_0}$, one merely applies the inverse wave map to every point on M_t to obtain the time-dependent invariant manifold $N^\pm_t$ for $V^t_{t_0}$. Note that, in the general case, $(\Omega^t_\pm)^{-1}$ is given by a limit, and one therefore

needs to consider convergence issues of computing $(\Omega_{\pm}^{t})^{-1}$. Bounds on the convergence of $(\Omega_{+}^{t})^{-1}$ can be obtained by Cooke's method, as used in Blazevski and de la Llave (2011). However, in the case the perturbation $\mathcal{P}(X,t)$ is compactly supported in time, $(\Omega_{\pm}^{t})^{-1}$ is not a limit and therefore there are no convergence issues in the case that $\mathcal{P}(X,t)$ is compactly supported in time (see Sec. II A for details).

A particular case of interest in this paper is when the flow $U_{t_0}^{t}$ is autonomous and subject to a time-dependent perturbation that is localized in time. The perturbed flow $V_{t_0}^{t}$ will therefore not in general have any of the classical structures that the flow $U_{t_0}^{t}$ has, namely fixed points, periodic orbits, KAM tori, etc. The existence of a conjugacy between the flows $U_{t_0}^{t}$ and $V_{t_0}^{t}$ may thus seem counterintuitive at first, but note that we have a *time-dependent* conjugacy. More precisely, suppose that M is an invariant manifold for the unperturbed flow $U_{t_0}^{t}$, for instance, a periodic orbit or a KAM torus. Although there are dynamics on the manifold M, the manifold itself is static. In contrast, for the perturbed flow, the wave maps yields time-dependent invariant manifolds N_{t_0} that are no longer static but the manifold itself is moving in time. Thus, even if the unperturbed manifold M is a classical object such as a fixed point or a periodic orbit, the corresponding object for the perturbed flow will now be a fixed point or a periodic orbit.

A. Compactly supported $\mathcal{P}$

Of particular interest is the case when $\mathcal{P}$ is compactly supported in time, that is, $\mathcal{P}(X,t)=0$ when $|t|>T$ for some $T>0$. In this framework, the wave maps always exist, and the case of laser-driven reaction considered in Sec. III has a compactly supported $\mathcal{P}$.

In this setting, it is interesting to compare our work with the recent work on transitory dynamics of Mosovsky and Meiss (2011). The setup and goals in Mosovsky and Meiss (2011) is similar to ours, though in Mosovsky and Meiss (2011), the consider vector fields of the form $\dot{X}=V(X,t)$ where

$$V(X,t)=\begin{cases} P(X) \text{ for } t<t_0 \\ F(X) \text{ for } t>t_1, \end{cases} \tag{9}$$

where $t_0<t_1$ and $P(X)$ represents the past dynamics and $P(X)$ represents the future dynamics and in the interval $[t_0,t_1]$, the vector field $V(X,\ t)$ can have arbitrary time-dependence. In Mosovsky and Meiss (2011), they use time-dependent invariant manifolds to understand finite-time transport. The setup of Blazevski and de la Llave (2011) takes the past and future dynamics to be the same, the past and future dynamics can be non-autonomous, and the past and future dynamics are linked via a perturbation that is localized in time that may not be compactly supported.

The numerical results in Sec. III are for the laser-driven Hénon-Heiles system first introduced in Kawai *et al.* (2007), which has a compactly supported perturbation. We chose this model since it is of physical interest and fits within the framework of scattering theory we use. However, from the computational perspective, a perturbation that is compactly supported in time is easier to work with. Indeed, if the perturbation $\mathcal{P}(X,t)$ is compactly supported in time, a limit is no longer needed to compute the wave maps. To see this, note that since $V_{\pm T}^{\pm t}=U_{\pm T}^{\pm t}$ for $|t|>T$, we have

$$\begin{aligned}\Omega_{\pm}^{t_0} &= \lim_{t\to\pm\infty} V_{\pm t}^{t_0}\circ U_{t_0}^{\pm t} = \lim_{t\to\pm\infty} V_{\pm T}^{t_0}\circ V_{\pm t}^{\pm T}\circ U_{\pm T}^{\pm t}\circ U_{t_0}^{\pm T} \\ &= V_{\pm T}^{t_0}\circ U_{t_0}^{\pm T}. \end{aligned} \tag{10}$$

Hence to compute the inverse wave map $(\Omega_{\pm}^{t_0})^{-1} = V_{\pm T}^{t_0}\circ U_{t_0}^{\pm T}$, which is needed to compute the perturbed invariant manifolds, one only needs to integrate trajectories for a finite specified time.

Moreover, Eq. (10) shows that no matter how large the amplitude $|\mathcal{P}(X,t)|$ of the perturbation is, the wave maps exist provided that $\mathcal{P}(X,t)$ is compactly supported in time. In case $\mathcal{P}(X,t)$ is not compactly supported, we believe that the methods of this paper can still be used to compute invariant manifolds, though one needs estimates on the convergence of the limits defining the wave maps.

As a simple example of the ideas developed thus far, consider the time-dependent perturbation of a 2D linear hyperbolic system

$$\begin{aligned}\dot{x} &= -x \\ \dot{y} &= \begin{cases} y+0.1e^{-(1.0-t^2)}e^{-x^2}, & \text{if } |t|<1 \\ y, & \textit{otherwise} \end{cases}. \end{aligned} \tag{11}$$

The perturbing term $0.1e^{-(1.0-t^2)}e^{-x^2}$ and all its derivatives vanish at $t=\pm 1$ and is peaked near $x=0$. Without the perturbation, the origin is a fixed point and the x-axis is its stable manifold. Using the time-dependent conjugacy (6), one obtains a family $N_{t_0}^{+}$ for the perturbed system shown in Figure 2. For $t_0 \ll -1$, the manifold approaches the x-axis as $t_0\to\infty$, and as $t_0\to -1$ and $t_0<-1$, the manifold moves away from the x-axis. Then for $-1<t_0<1$, the manifold starts to go back to the x-axis and for $t_0>1$ the manifold simply is the x-axis. The manifold is furthest from the x-axis when $t_0=-1$ since for $t_0>-1$ the perturbation has had its full effect yet, and for $t_0<-1$, the manifold starts to hyperbolic dynamics kick back in and the manifolds relaxes back to the x-axis.

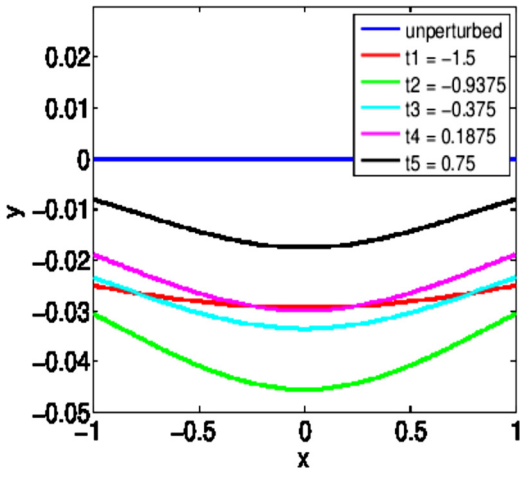

FIG. 2. Time-dependent family of manifolds for the perturbation of a 2D hyperbolic linear system (11).

B. Asymptotic and eventually fixed points, periodic orbits, and KAM tori

We further explore the implications the existence of the wave maps has on the dynamics of the perturbed system. Suppose one has a classical invariant object such as a fixed point, a periodic orbit, a KAM torus, etc. Then, in the perturbed systems, there are no such structures, however, the corresponding objects that we can compute using scattering theory for the perturbed system will be *asymptotically* fixed points, periodic orbits, and KAM tori.

Indeed, suppose that X_0 is an initial condition of a fixed point, a periodic orbit, or a KAM torus. Then the points X_0^+ (for the asymptotic future) and X_0^- (for the asymptotic past) defined by

$$X_0^{\pm} = (\Omega_{\pm}^{t_0})^{-1}(X_0) \tag{12}$$

are initial conditions for asymptotically fixed points, periodic orbits, and KAM tori in the past and present. The time-dependent conjugacy (6) tells us that the dynamics is conjugate to the dynamics of X_0. Moreover, simply by the definition of the wave maps, the perturbed orbit itself is asymptotic to the unperturbed orbit that is if γ is the unperturbed orbit then

$$\lim_{t_0\to\infty} d(\gamma, \{V_{t_0}^t(X_0^+) : t > t_0\}) = 0,$$
$$\lim_{t_0\to-\infty} d(\gamma, \{V_{t_0}^{-t}(X_0^-) : t < t_0\}) = 0. \tag{13}$$

See Figure 3 for a geometric representation of asymptotically periodic orbits.

In the special case when $\mathcal{P}(X,t)$ is compactly supported in time, instead of asymptotic fixed points, periodic orbits, and KAM tori, we have something even stronger, namely eventually fixed points, periodic orbits, and KAM tori. Suppose that X_0 is an initial condition for a fixed point, a periodic orbit or a KAM torus for the unperturbed flow $U_{t_0}^t$ and consider the points $X_0^{\pm} = (\Omega_{\pm}^{t_0})^{-1}(X_0)$. If the perturbation $\mathcal{P}$ is supported in the interval $[-T, T]$, we saw in Sec. II A that the wave maps are not in fact limits, namely, we have

$$X_0^{\pm} = V_{\pm T}^{t_0} \circ U_{t_0}^{\pm T}(X_0). \tag{14}$$

Thus, $V_{t_0}^{\pm T}(X_0^{\pm}) = U_{t_0}^{\pm T}(X_0)$ is on the unperturbed orbit, which is to say that if we flow X_0^+ forward in time from t_0 to T, the trajectory lands on the unperturbed trajectory, and since $\mathcal{P} = 0$ for $t \geq T$, after time T the perturbed trajectory will follow the unperturbed trajectory, but behaves unpredictably for $t < T$. Similarly, flowing X_0^- backward in time to $t = -T$ lands us on the unperturbed trajectory and the orbit is the same as the unperturbed orbit if we continue to flow further backward in time.

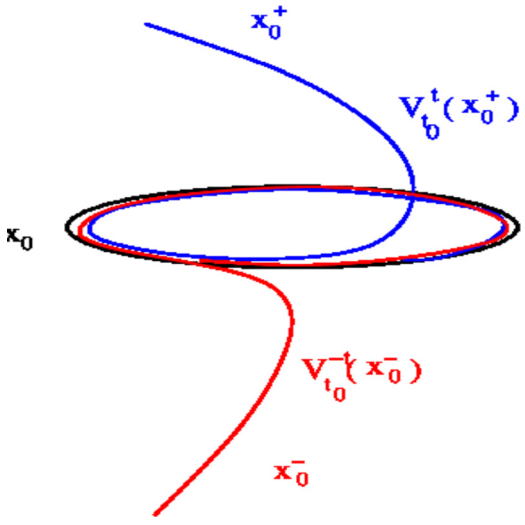

FIG. 3. Depiction of an asymptotically periodic orbit. The point X_0 is an initial condition for a periodic orbit (in black) for the unperturbed flow $U_{t_0}^t$. The points $X_0^{\pm} := (\Omega_{\pm}^{t_0})^{-1}$ are initial conditions for asymptotically periodic orbits in the future (corresponding to X_0^+ in blue) and past (corresponding to X_0^- in red).

III. RESULTS FOR THE LASER-DRIVEN HÉNON-HEILES SYSTEM

In this section, we apply the theory developed in Sec. II to the laser-driven Hénon-Heiles system introduced in Kawai *et al.* (2007). The motivation for computing invariant manifolds for models appearing in chemistry is transition state theory, which has achieved recent progress to compute rates of reactions by computing invariant manifolds that separate the regions of phase space that lead to a certain outcome of a reaction. (See, for example, Bartsch *et al.* (2012); Gabern *et al.* (2005); Haller *et al.* (2011); Waalkens *et al.* (2008).) In this section, we focus on how to numerically compute invariant manifolds for molecules subject to a laser for a short time.

We consider the laser-driven Hénon-Heiles system whose Hamiltonian is given by

$$H(x,y,p_x,p_y) = \frac{1}{2}(p_x^2+p_y^2) + \frac{1}{2}(x^2+y^2) + x^2y - \frac{1}{3}y^3 + \mathcal{E}_1(t)\exp(-\alpha x^2 - \beta y^2), \tag{15}$$

where

$$\mathcal{E}_1(t) = -\frac{\partial}{\partial t}A(t) \tag{16}$$

and

$$A(t) = \begin{cases} -A_0\cos^2\left(\frac{\omega t}{2N}\right), & \text{if } |t| < \frac{N\pi}{\omega} \\ 0, & \textit{otherwise}. \end{cases} \tag{17}$$

The term $\mathcal{E}_1(t)$ is a perturbation that represents shining a laser on the molecules for a short time and the values for the remaining variables have been chosen in accordance with the system used in Kawai *et al.* (2007), namely, we take $\alpha = 2, \beta = 4, \omega = 3, N = 4$, and $A_0 = \frac{1}{30}$. Thus, the perturbation is zero for $|t| > 4.189$.

For the unperturbed system, we have the well known invariant objects of the Hénon-Heiles system that we consider, which include fixed points, periodic orbits, and their stable and unstable manifolds. We focus our attention to two energy values $e = 1/12$ and $e = 1/6$. Fixing the energy to either of

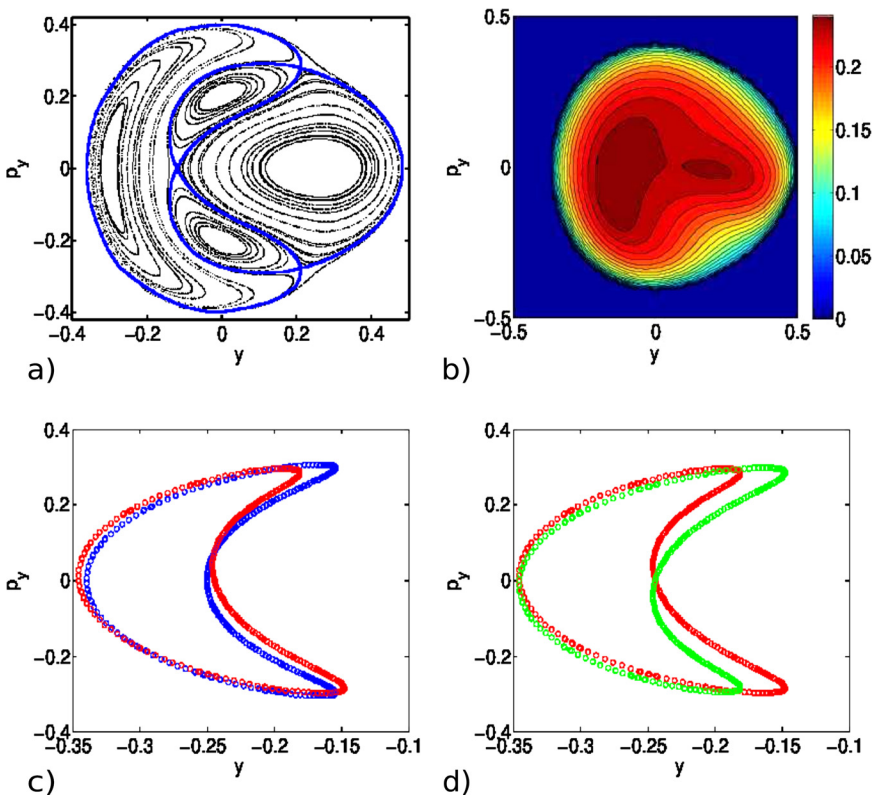

FIG. 4. The Poincare plot for $e = 1/12$ is shown in (a). A contour plot of the function D that computes the distance between the inverse wave map $(\Omega_+^{t_0})^{-1}$ and the identity is shown in (b) for $t_0 = -4.2$. In (c), we compare an unperturbed trajectory for the Poincare map (in blue) and the perturbed trajectory for $t_0 = -4.2$ (in red). Finally, in (d), we reflected the unperturbed trajectory for $t_0 = -4.2$ about the y-axis and noticed a lack of symmetry about the y-axis of the unperturbed trajectories.

these values, and taking the surface of section $x = 0$ leads to the well known Poincare plots seen in Figures 4(a) and 7(a).

For $e = 1/12$, there are three hyperbolic fixed points for the Poincare map corresponding to hyperbolic periodic orbits of the flow, each of which was computed using Newton's method for the function

$$F(y, p_y) = P(y, p_y) - \mathrm{Id}(y, p_y), \tag{18}$$

where $P(y, p_y)$ is the Poincare map and Id is the identity map. Initial guesses were gathered from the Poincare plot, and the three hyperbolic fixed points are $(y_1, p_{y_1}) = (-0.1203..., 0.0)$, $(y_2, p_{y_2}) = (0.2110..., 0.2780...)$, and $(y_3, p_{y_3}) = (0.2110..., -0.2780...)$.

We also computed the stable and unstable manifolds using a method based on linearizing the Poincare map at the fixed points. First, the Jacobian matrix $DP(y_0, p_{y0})$ was computed for each fixed point (y_0, p_{y_0}). Since the fixed points are hyperbolic, there are stable and unstable eigenvalues λ^s and λ^u with $|\lambda^s| < 1$ and $|\lambda^u| > 1$ and corresponding eigenvectors $v^s := (v_y^s, v_{p_y}^s)$ and $v^u := (v_y^u, v_{p_y}^u)$. Since $v^{s,u}$ are tangent to W_u^s at (y_0, p_{y_0}), a small perturbation is added to each fixed point in the direction of the respective stable or unstable eigenvector. The eigenvectors are scaled in both the positive and negative directions to account for the fact that hyperbolic fixed points have two incoming stable manifolds and two outgoing unstable manifolds. Thus, for $0 < \varepsilon \ll 1$, the points

$$\begin{aligned}(y_s, p_{y_s}) &= (y_0 \pm \varepsilon v_{y_0}^s, p_{y_0} \pm \varepsilon v_{p_{y_0}}^s),\\ (y_u, p_{y_u}) &= (y_0 \pm \varepsilon v_{y_0}^u, p_{y_0} \pm \varepsilon v_{p_{y_0}}^u)\end{aligned} \tag{19}$$

are approximately on W^s and W^u, respectively. The manifolds are then calculated by iterating $P(y_u, p_{y_u})$ for the unstable manifold and $P^{-1}(y_s, p_{ys})$ for the stable manifold. This gives one trajectory that is approximately on the stable or unstable manifolds, and the remainder of the manifold was obtained by interpolation. The stable and unstable manifolds of each of the three fixed points in Figure 4 are shown in thick blue (color on line only). Note that we have heteroclinic connections between different fixed points.

To understand what happens to the structure of the phase space for the perturbed laser-driven system, it is natural to be primarily interested in objects for a starting time t_0 just before the onset of the laser pulse and flow the forward until after the laser is turned off. Thus, since $\Omega_+^{t_0}$ give the forward dynamics of the perturbed system, the relevant invariant objects of the perturbed system were computed by applying the inverse wave map

$$(\Omega_+^{t_0})^{-1} = V_{t_f}^{t_0} \circ U_{t_0}^{t_f}, \tag{20}$$

to every point on the corresponding unperturbed object for t_0 in the interval $[-5.0, 5.0]$. One can also consider past dynamics and the wave map $\Omega_-^{t_0}$, but the results are similar and of less interest physically.

Figure 4(b) shows the how far the perturbed points move by computing the difference between the wave map and the identity

$$D = ||(\Omega_+^{t_0})^{-1} - \mathrm{Id}||. \tag{21}$$

Figure 4(b) shows the contour plot of D on the domain of the Poincare map. It is important to the remark that the distance D is computed in the *full phase space*, not simply in the y-p_y plane. More precisely, to each point (y, p_y) in the domain of the Poincare map, we have a corresponding point

$X = (x, y, p_x, p_y) = (0.0, y, p_x(y, p_y), p_y)$ in the full phase space, where we are using the fact that fixing an energy value e_0 and $x = 0$ allows us to compute $p_x(y, p_y) = \sqrt{-p_y^2 - y^2 + 2/3y^3 + 2e_0}$ as a function of y and p_y. The wave map $\Omega_+^{t_0}$, the identity function and the distance defining D are then computed using the points in full phase space. Since the perturbation is localized near the origin in the full phase space, it is expected that D is peaked near $(y, p_y) = 0$, which is indeed what we observe.

To further understand the difference between the perturbed and unperturbed systems, we took a single orbit $(y, p_y) = (-0.25, 0.0)$ of the Poincare map and computed the inverse wave map $(\Omega_+^{t_0})^{-1}$ to each point on the orbit and plotted the result in the y-p_y plane. The result is shown in Figure 4(c).

The unperturbed Hénon-Heiles system has many symmetries, one in particular is symmetry about $\{y = 0\}$. The perturbation breaks the symmetry and the unperturbed orbits are not symmetric like their perturbed counterparts. This is shown in Figure 4(d) where we plot the perturbed orbit in the y-p_y plane and the reflection of the orbit about the horizontal axis.

As we emphasized in Secs. I and II, invariant stable and unstable manifolds are of interest in chemistry since they separate regions of phase space leading to different outcomes of a chemical reaction and can be used to compute reaction rates. Thus, an important question to ask is what happens to unperturbed manifolds in the laser-driven system. We took the heteroclinic arcs connecting the fixed points $(y_1, p_{y_1}) = (-0.1203..., 0.0)$ and $(y_2, p_{y_2}) = (0.2110..., 0.2780...)$, and computed the corresponding time-dependent invariant forward manifolds $N_{t_0}^+$ for the perturbed system are computed for t_0 in the interval $[-5.0, 5.0]$. This time interval is chosen since the laser term in the Hamiltonian is supported in $[-4.189, 4.189]$. Thus, we compute the manifolds starting at a time before the laser pulse, and see how they evolve forward in time until just after the laser is turned off. Computing $N_{t_0}^+$ was computed by applying the inverse wave map $(\Omega_+^{t_0})^{-1}$ to each point on the unperturbed manifold for different times t_0. The result is shown in Figure 5.

One can also carry out similar computation for a different energy value. The energy value $e = 1/6$ is a critical value of the energy, and we obtain interesting results due to criticality. The criticality of the energy value $e = 1/6$ has been considered before in Arioli and Zgliczyński (2003), and the criticality lies in the fact that there is no well-defined Poincare map for the section $x = 0$ and energy value $e > 1/6$. In Figures 6(a) and 6(b), the closed curves in the middle shows the domain of the Poincare map, and in Figure 6, we see that for $e > 1/6$ there is no curve that confines many of the points to stay within a bounded region. For $e > 1/6$, there still may be elliptic islands near $(y, p_y) = (0.0, 0.0)$ and $(y, p_y = 0.5, 0.0)$ corresponding to the islands for energy $e = 1/6$ seen in Figure 7(a) that have confined orbits, but the chaotic regions in Figure 7(a) will not be confined once we take $e > 1/6$.

For the $e = 1/6$ case, the hyperbolic fixed point $(y, p_y) = (1, 0)$ is degenerate for the Poincare map since it is actually a fixed point for the flow and hence never leaves y-p_y plane. For $t_0 = -4.2$, we compute the perturbed trajectories near one of the unperturbed elliptic islands, and we again observe a definite lack of symmetry about the y-axis.

Because the energy value $e = 1/6$ is a critical value of the energy, if the perturbed orbits increase in energy as the laser turns on, the orbits can escape to infinity. This happens to the degenerate fixed point $(y, p_y) = (1.0, 0.0)$ as seen in Figure 7(c), which tracks $||(\Omega_+^{t_0})^{-1}(X_0) - X_0||$ where $X_0 = (0.0, 1.0, 0.0, 0.0)$. Thus, the forward dynamics of the

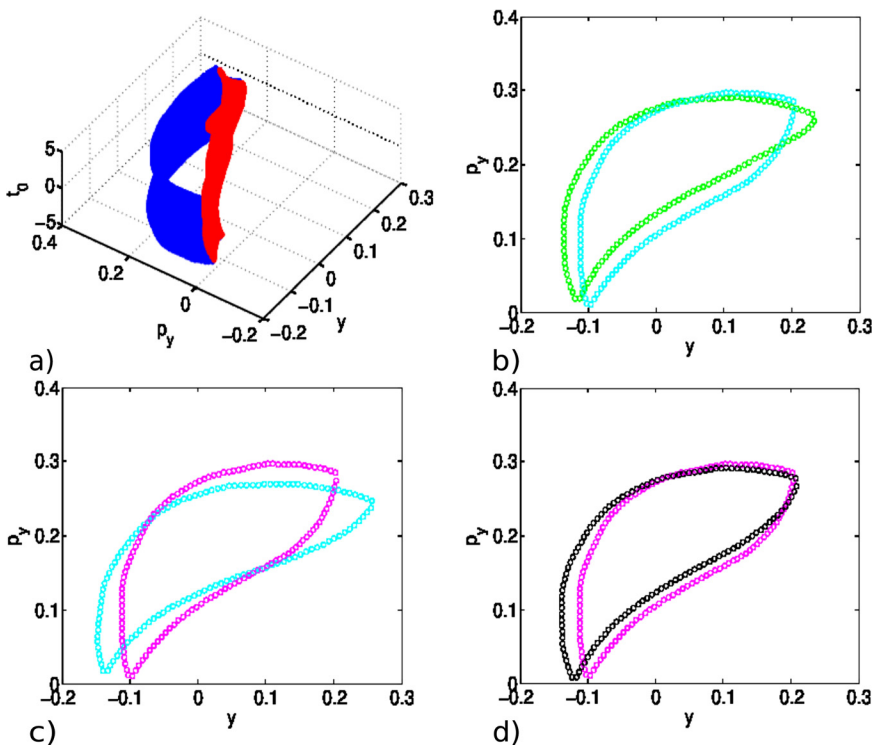

FIG. 5. The behavior of the invariant manifolds over time for $e = \frac{1}{12}$ is considered in (a) by computing $(\Omega_+^{t_0})^{-1}$ of a manifold for t_0 values in [–5.0, 4.0]. (b)–(d) show the manifolds for different times, namely, $t_0 = -5$ (in green), $t_0 = -2$ (in cyan), $t_0 = 1$ (in magenta), and $t_0 = 4$ (in black).

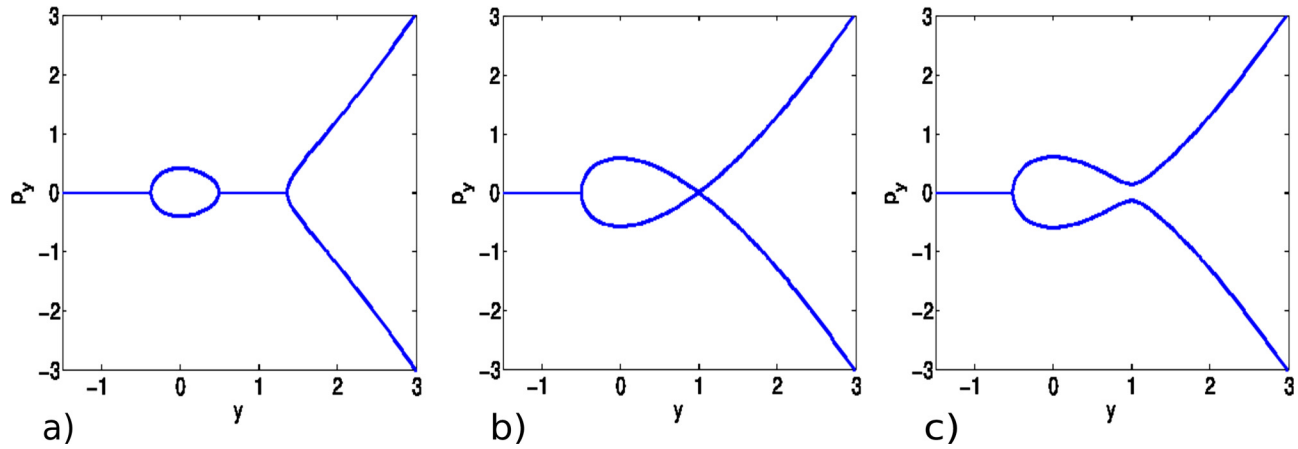

FIG. 6. Bifurcation of the regions where the Poincare map is defined for energies: (a) $e = 1/12$, (b) $e = 1/6$, (c) $e = 1/6 + 0.001$. The energy value $e = 1/6$ is a critical value of energy since orbits for $e = 1/6 + 0.001$ escape to infinity.

trajectory corresponding to X_0 for the perturbed flow is at infinity when $t_0 = -\infty$ and moves in closer to the fixed point and lands on the unperturbed fixed point when the laser is turned off at $t = 4.189$ and stays there after the laser is turned off. Note that although c) shows that the orbit comes from infinity, if we compute the change in energy along the orbit

$$\Delta E = |H_0 \circ (\Omega_+^{t_0})^{-1} - H_0|, \tag{22}$$

where H_0 is the unperturbed Hénon-Heiles Hamiltonian, we see that the energy along the orbit is remarkably close the $e = 1/6$, the energy of the fixed point.

As expected, we found that the energy does not change much generically, even though the orbits may escape to infinity under the perturbed system. We computed the change in energy by computing ΔE using Eq. (22), and made contour plots for $e_0 = 1/12$ and $e = 1/6$. The result is shown in Figure 8, and we indeed see little change in energy, especially when compared to the actual distance moved in phase space.

Lastly, we can compute eventually periodic orbits described in Sec. II. We consider periodic orbit for energy $e = 1/12$ corresponding to the point $(y_1, p_{y_1}) = (-0.1203..., 0.0)$ on the Poincare plot in Figure 4(a). In Figure 9(a), we plot the evolution of the orbit under the unperturbed flow in the y-p_y plane. Taking $X_0 = (0.0, -0.1203..., 0.3886..., 0.0)$ as an initial condition for the unperturbed orbit, we computed $X_0^+ = (\Omega_+^{t_0})^{-1} = V_T^{t_0} \circ U_{t_0}^T(X_0)$ for $t_0 = -4.2$. For t in the interval $[t_0 = -4.2, T]$, the laser is on and the orbit is behaving unpredictably. However, the instant the laser is turned off

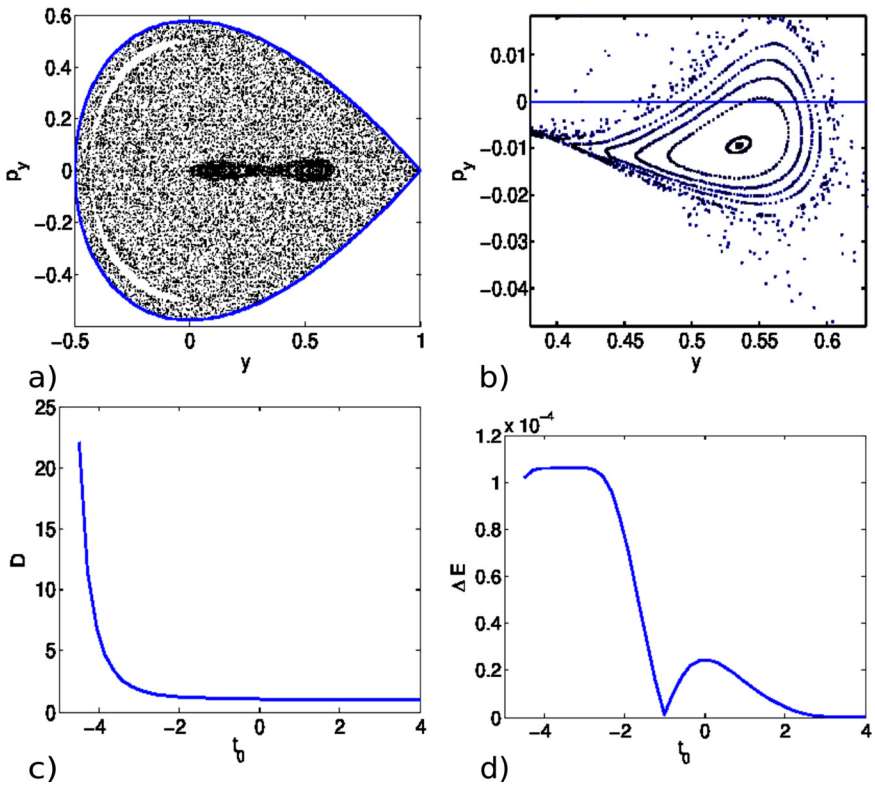

FIG. 7. The Poincare plot for the unperturbed system is shown in (a). If we apply the inverse wave map $(\Omega_+^{t_0})^{-1}$ for $t_0 = -4.2$ to the orbits near one of the elliptic islands we obtain the asymmetric (w.r.t the y-axis) unperturbed time-dependent manifolds at time $t_0 = -4.2$ shown in (b). (c) The distance $D = ||(\Omega_+^{t_0})^{-1}(X_0) - X_0||$ from the unperturbed fixed point $X_0 = (0.0, 1.0, 0.0, 0.0)$ as a function of t_0 and (d) plots $\Delta E = |H_0(\Omega_+^{t_0})^{-1}(0.0, 1.0, 0.0, 0.0) - 1/6|$ as a function of t_0.

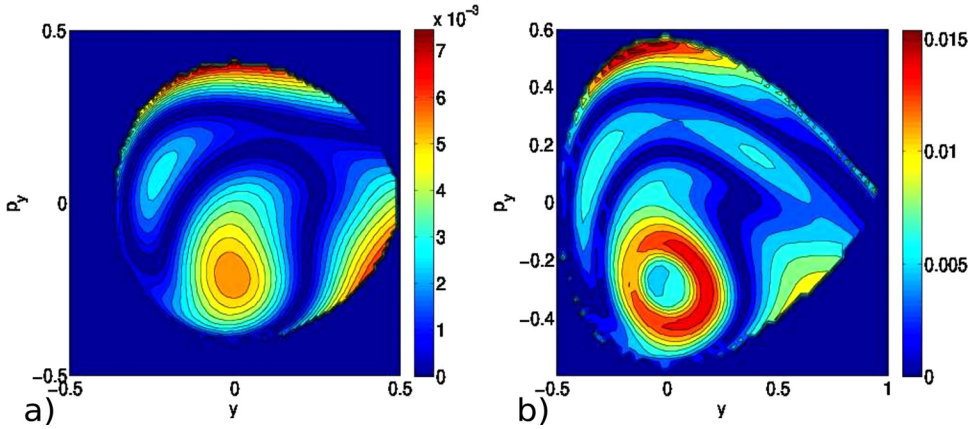

FIG. 8. A change in energy between the unperturbed and perturbed systems was computed for $e = \frac{1}{12}$ in (a) and for $e = \frac{1}{6}$ in (b) for $t_0 = -2.0$.

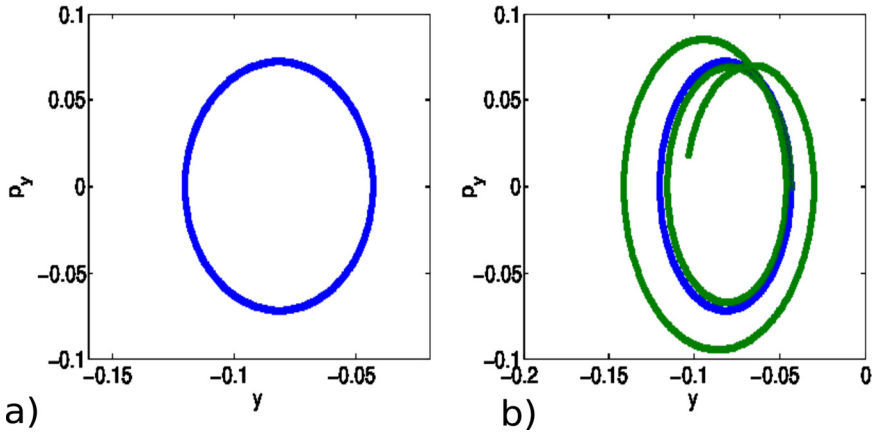

FIG. 9. Periodic unperturbed orbit in (a) and the corresponding eventually periodic orbit for the perturbed system in (b).

at $t = T$ we have $V^t_{t_0}(X_0^+) = U^T_{t_0}(X_0)$ and hence the orbit lands on the unperturbed periodic orbit once the laser is off and for $t > T$ the flow of $V^t_{t_0}$ agrees with $U^t_{t_0}$ and therefore the orbit is periodic forward in time for $t > T$.

IV. CONCLUSION

In this paper, we described how to implement numerically the ideas developed in Blazevski and de la Llave (2011). We considered the specific example of the laser-driven Hénon-Heiles system introduced in Kawai *et al.* (2007). Using the time-dependent conjugacy given by the intertwining relations, we reduced the computation of time-dependent invariant manifolds for the laser-driven system to applying the inverse wave maps $(\Omega^{t_0}_{\pm})^{-1}$ to the unperturbed invariant manifolds. In particular, we do not use time-dependent normal form theory use in Kawai *et al.* (2007). In the case, the perturbation is compactly supported in $[-T, T]$, one merely needs to apply the transformation

$$(\Omega^{t_0}_{\pm})^{-1} = V^{t_0}_{\pm T} \circ U^{\pm T}_{t_0}, \tag{23}$$

to each point on the unperturbed manifold. Thus, one can use whatever methods one likes to compute the unperturbed objects and then apply $(\Omega^{t_0}_{\pm})^{-1}$ to each point on the unperturbed manifold. With respect to points on the unperturbed manifold and modifying t_0, our method is highly parallelizable.

ACKNOWLEDGMENTS

Both the authors are indebted to Professor R. de la Llave for suggesting the project, and helping to start a collaboration between the authors. Both authors have been supported by NSF Grant No. DMS0901389 and the Texas Coordinating Board ARP0223.

Arioli, G. and Zgliczyński, P., "The Hénon-Heiles Hamiltonian near the critical energy level—some rigorous results," Nonlinearity **16**, 1833–1852 (2003).
Bartsch, T., Revuelta, F., Benito, R. M., and Borondo, F., "Reaction rate calculation with time-dependent invariant manifolds," J. Chem. Phys **136**(22), 224510 (2012).
Blazevski, D. and de la Llave, R., "Time-dependent scattering theory for odes and applications to reaction dynamics," J. Phys. A: Math. Theor. **44**, 195101 (2011).
Gabern, F., Koon, W. S., Marsden, J. E., and Ross, S. D., "Theory and computation of non-RRKM lifetime distributions and rates in chemical systems with three or more degrees of freedom," Physica D **211**, 391–406 (2005).
Gutkin, E., "Asymptotics of trajectories for cone potentials," Physica D **17**, 235–242 (1985a).
Gutkin, E., "Integrable Hamiltonians with exponential potential," Physica D **16**, 398–404 (1985b).
Haller, G., Uzer, T., Palacián, J., Yanguas, P., and Jaffé, C., "Transition state geometry near higher-rank saddles in phase space," Nonlinearity **24**, 527–561 (2011).
Hubacher, A., "Classical scattering theory in one dimension," Commun. Math. Phys. **123**, 353–375 (1989).

Kawai, S., Bandrauk, A. D., Jaffe, C., Bartsch, T., Palacian, J., and Uzer, T., "Transition state theory for laser-driven reactions," J. Chem. Phys. **126**, 164306 (2007).

Mosovsky, B. A. and Meiss, J. D., "Transport in transitory dynamical systems," SIAM J. Appl. Dyn. Syst. **10**, 35–65 (2011).

Nelson, E., *Topics in Dynamics. I: Flows*, Mathematical Notes (Princeton University Press, Princeton, NJ, 1969), pp. iii+118.

Waalkens, H., Schubert, R., and Wiggins, S., "Wigner's dynamical transition state theory in phase space: Classical and quantum," Nonlinearity **21**, R1–R118 (2008).